Applied Physics A (2025) 131:285
https://doi.org/10.1007/s00339-025-08366-5

Data-driven characterization of plastic deformation and mechanical properties in hot-pressed Ti/Al/Ti laminates

Mohamed Sharaf[1] · Nikunj Rachchh[2] · T. Ramachandran[3] · Aman Shankhyan[4] · Vikasdeep Singh Mann[5] · Mohammed El-Meligy[6,7]

Received: 7 January 2025 / Accepted: 22 February 2025

Abstract
This study investigates the prediction and evaluation of mechanical characteristics in hot-pressed Ti/Al/Ti laminates using a Random Forest (RF) machine learning model. The training dataset was generated through numerical simulations, encapsulating the laminates' complex mechanical behavior under diverse conditions. To optimize model performance, hyperparameter tuning techniques, including Grid Search (GS), Particle Swarm Optimization (PSO), and Genetic Algorithms (GA), were applied. Among these, the GA-tuned RF model exhibited the highest predictive accuracy, achieving R^2 values of 0.947 for yield stress, 0.937 for yield strength, and 0.928 for Poisson's ratio. The superior performance of the GA-tuned model is attributed to its effective feature selection and optimization capabilities, surpassing GS and PSO by identifying the most relevant input features. Relevance score analysis also revealed a balanced contribution of material geometry (e.g., thickness) and pressing parameters for predicting yield stress and ultimate strength, while induced strain played a significant role in predicting Poisson's ratio. A case study using the GA-RF model further unveiled intricate relationships between input variables and mechanical properties, providing valuable guidance for optimizing hot-pressing parameters to enhance laminate performance.

Keywords Hot pressing · Ti/Al/Ti laminates · Mechanical properties · Machine learning · Hyperparameter tuning · Numerical simulation

1 Introduction

Titanium-aluminum laminated composites have emerged as significant materials in advanced engineering applications, owing to their remarkable balance of lightweight, high strength, and excellent corrosion resistance [1–3]. The layered structure of Ti/Al composites effectively combines titanium's strength, ductility, and resilience with aluminum's low density and superior thermal and electrical conductivity. This synergistic approach in composite production not only boosts mechanical performance but also enhances energy absorption and reduces crack propagation, providing a material solution that outperforms traditional monolithic materials [4–6]. Achieving the desired properties in Ti/Al laminated composites requires precise control over the production process. Various methods, such as diffusion bonding, explosive welding, and accumulative roll bonding, have been explored for creating these laminates [7, 8]. Among these, hot pressing has also emerged as an effective and versatile technique for fabricating high-quality

✉ Aman Shankhyan
aman_shankhyan@outlook.com;
amanshankhyan53@gmail.com

1 Industrial Engineering Department, College of Engineering, King Saud University, Riyadh 11421, Saudi Arabia

2 Department of Mechanical Engineering, Faculty of Engineering & Technology, Marwadi University, Rajkot, Gujarat 360003, India

3 Department of Mechanical Engineering, School of Engineering and Technology, JAIN (Deemed to be University), Bangalore, Karnataka, India

4 Department of Mechanical Engineering, University of Bridgeport, Bridgeport CT 06604, USA

5 Department of Mechanical Engineering, Chandigarh Engineering College, Chandigarh Group of Colleges-Jhanjeri, Mohali140307, Punjab, India

6 Jadara University Research Center, Jadara University, PO Box 733, Irbid, Jordan

7 Applied Science Research Center, Applied Science Private University, Amman, Jordan

Published online: 18 March 2025

Ti/Al composites. Hot pressing involves applying heat and pressure simultaneously to bond the dissimilar layers, enabling strong metallurgical bonding while minimizing defects [9, 10]. By operating at elevated temperatures, the process promotes diffusion at the interface, ensuring excellent adhesion between layers. Experimental studies have extensively explored the performance and properties of Ti/Al laminates under various conditions in the hot pressing. For instance, one study demonstrated that hot-pressed Ti/Al sheets exhibit remarkable ductility at elevated temperatures, achieving an elongation of 135% at 600 °C [11]. Another investigation by Que et al. [12] revealed that optimizing process parameters, such as grain size and recrystallization fraction, led to the formation of nanoscale $TiAl_3$ phases with significant stacking faults, enhancing interfacial bonding and mechanical strength. Additionally, hierarchical modifications to bimodal grain structures were shown to achieve an exceptional strength-ductility synergy in Ti/Al laminates [13]. Recent advancements in this field also include integrating high-entropy alloy particles and ultrasonic consolidation into the fabrication process of Ti/Al laminates, which further improve tensile strength, crack resistance, and anisotropic flexural properties of these composites [14, 15].

Beyond experimental efforts, finite element (FE) simulations have emerged as a powerful tool for analyzing the behavior of hot-pressed Ti/Al laminates. Such studies affirm that FE analysis is a powerful tool for evaluating the plasticity and mechanical properties of Ti/Al laminates. Moreover, similar studies have effectively utilized FE analysis to investigate the behavior of laminates under hot pressing, demonstrating its reliability for understanding and optimizing processing conditions [16, 17]. However, despite their utility, FE simulations can be computationally intensive and time-consuming, particularly when applied to large datasets or real-time predictions [18, 19]. These limitations underscore the need for complementary approaches to enhance efficiency without compromising accuracy. In this regard, machine learning (ML) offers a promising alternative to traditional simulation-based methods. ML models excel in processing large datasets, identifying complex patterns, and delivering rapid predictions, making them particularly well-suited for material property evaluations [20–22]. Considering the context of this work, ML has demonstrated exceptional potential for predicting mechanical responses and plasticity behavior under various processing conditions, including laminated composites [23, 24], and hot pressing processes [25, 26].

Building on existing literature, this study proposes a novel hybrid approach that integrates FE simulations with ML techniques to improve the prediction, understanding, and optimization of hot-pressed Ti/Al/Ti laminates. Recent advancements in materials science have also demonstrated the potential of ML-FE integration for accurately and efficiently predicting the mechanical responses of various materials and structures [27–29]. In this work, FE simulations serve as the primary data source, generating a comprehensive and reliable dataset. This dataset is then used to train ML models, enabling precise and efficient predictions of mechanical responses in laminated composites. The proposed approach introduces several key novelties and advantages. By combining FE-generated data with ML models, this study achieves a unique balance between high-fidelity simulation results and rapid predictive capabilities. Furthermore, the proposed model uncovers complex relationships between processing parameters and mechanical properties that conventional numerical methods often fail to capture. This deeper insight facilitates the optimization of hot-pressing parameters, enabling the development of Ti/Al/Ti laminates with tailored mechanical properties for advanced engineering applications. Additionally, the framework is scalable and adaptable, allowing for continuous integration of new data, making it applicable to a broad range of material systems and processing conditions. From an ML perspective, this study also demonstrates how proper hyperparameter tuning significantly enhances predictive accuracy in materials property estimation. Ultimately, this work contributes to both materials science and ML implementation, advancing the field of hot-pressed laminate production through a data-driven approach.

2 Methodology

2.1 Numerical simulation as a data collection method

In this study, numerical simulations were conducted to generate data on the hot pressing of Ti/Al/Ti laminates, which were subsequently used for training ML models. Specifically, FE simulations were carried out using Abaqus, incorporating a thermo-displacement approach to accurately represent the coupled thermal and mechanical behavior during the pressing process. The thermo-displacement approach in the simulation modeled the interaction between thermal and mechanical fields [30]. As the laminate was subjected to heat and pressure, the thermal field influenced the mechanical deformation by altering the materials' yield strength and elastic modulus. Conversely, the mechanical deformation affected heat transfer by changing contact areas and conduction paths. This bidirectional coupling was critical for accurately capturing the evolution of stresses, strains, and temperature gradients during the hot pressing of Ti/Al/Ti laminates. The Ti/Al/Ti configuration was modeled with varying layer thicknesses, where the bonding between

titanium and aluminum layers was done through the existence of intermetallic $TiAl_3$ at the interfaces. The metallic layers were characterized as elastoplastic to capture their ability to undergo plastic deformation under applied loads, while the $TiAl_3$ intermetallic, known for its brittle behavior, was modeled as an elastic material. This distinction ensured realistic representation of the material behavior under pressing conditions.

As seen in Fig. 1a, the simulation utilized a thermally coupled, 8-node element with trilinear displacement and temperature capabilities and reduced integration (C3D8T). This element was chosen for its ability to efficiently and accurately represent the thermal-mechanical interactions in complex processes like hot pressing. The choice of C3D8T elements ensured that the thermal and mechanical responses were simultaneously computed, accounting for temperature-dependent material behavior such as softening in the metallic layers and thermal expansion mismatches at the interfaces. Moreover, the $TiAl_3$ interface was explicitly meshed using the same C3D8T elements as the metallic layers to ensure compatibility in temperature and displacement calculations, eliminating the need for additional contact definitions. To ensure a realistic representation of boundary conditions, the nodes located on the bottom tray were constrained along the X-axis, effectively restricting any lateral movement. Additionally, the interfacial bonding between Ti, $TiAl_3$, and Al was enforced by constraining the displacement degrees of freedom at shared nodes, ensuring perfect adhesion without requiring separate cohesive elements. A reference point was defined on the top of the upper tray, allowing the capture of force and displacement data during the simulation. The pressing action was simulated by incrementally displacing the top tray, with data recorded at each step to analyze the pressing force requirements and deformation behavior of the laminate. Hot pressing was simulated over a wide range of processing parameters, including varying temperatures, pressing durations, and pressing pressure. This comprehensive parameter set enabled the analysis of the laminate's response under different conditions, providing a robust dataset for subsequent ML training.

A representative volume element (RVE) with dimensions of 5 mm × 5 mm × 5 mm was constructed to investigate material behavior at the microscale (See Fig. 1b). The RVE consisted of alternating titanium and aluminum layers with $TiAl_3$ interfaces, maintaining geometric symmetry to reduce computational demands while preserving

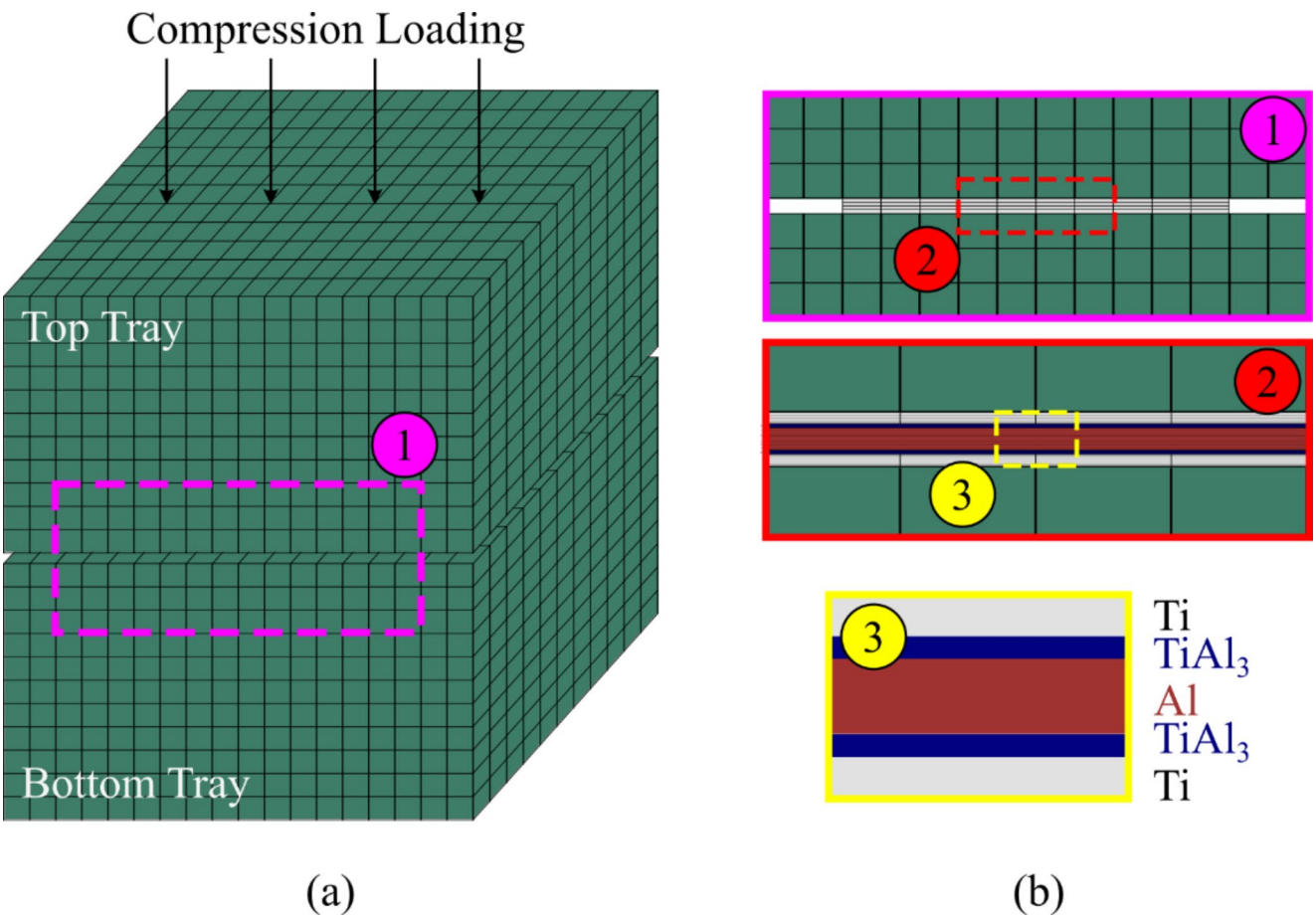

Fig. 1 (**a**) Schematic of the tray/sample configuration used in the pressing process, (**b**) Representative Volume Element model for analysis

the physical accuracy of the model. Symmetric boundary conditions (SBC) were also applied to constrain the edges of the RVE, ensuring periodicity in deformation and stress distribution [31]. Following the hot pressing simulation, a tensile test was modeled to evaluate the mechanical properties of the Ti/Al/Ti laminate. The test setup involved applying a uniaxial tensile load perpendicular to the laminate's plane to assess its strength and ductility. The strain rate was set to 10^{-3} s^{-1} to simulate quasi-static conditions, ensuring that the material response was not influenced by strain rate effects. In the simulation, the bottom nodes of the laminate were fixed to prevent movement, creating a stable boundary condition. A controlled displacement was applied to the top nodes, mimicking the experimental tension test. A reference point was defined on the top surface to monitor the force-displacement response throughout the simulation.

2.2 Data identification and extraction for model training

In this study, several parameters from the FE simulation were selected as inputs for the ML training process. These input features included the thickness of the Al layer (D_{al}=1.5–3.5 mm), the thickness of Ti layers (D_{ti}=1.5–3.5 mm), the intermetallic layer thickness (D_{im}=0–0.1 mm), the pressing temperature (T = 670–820 K), the pressing time (t = 10–30 min), and the pressing pressure (L = 30–60 MPa). These parameters were chosen to capture a wide range of processing conditions and material configurations, ensuring that the training dataset adequately represented the variability in the process. Figure 2a provides an example of the stress and strain distribution in a pressed Ti/Al/Ti laminate sample. The maximum stress is observed at the intermetallic/Ti boundaries, likely due to the mismatch in elastic modulus and thermal expansion coefficients between the intermetallic $TiAl_3$ layer and the Ti layers. This mismatch creates localized stress concentrations under pressing pressure. Conversely, the maximum induced strain occurs at the Al/intermetallic boundaries, which can be attributed to the lower yield strength and higher ductility of the aluminum compared to the intermetallic and titanium layers. This mechanical incompatibility leads to significant strain accumulation near the softer aluminum layer. Based on these insights, the maximum stress (σ_{max}) and strain (ε_{max}) at the interfacial boundaries, as well as the average values of stress (σ_{ave}) and strain (ε_{ave}) across the volume of each layer, were selected as additional input features for the ML model. These features provide a detailed description of the mechanical behavior within the laminate under hot pressing conditions. Figure 2b and c illustrate the mechanical behavior of a sample subjected to tensile loading. Figure 2b displays the distribution of induced strain across the laminate layers, emphasizing the plastic deformation occurring in the aluminum and titanium layers. The strain concentration in the aluminum layer can be attributed to its higher ductility compared to the titanium layers. Figure 2c shows the corresponding stress-strain curve obtained from the tensile test, highlighting critical mechanical properties such as the yield stress (σ_y) and ultimate tensile strength (σ_u), which are key indicators of the material's ability to withstand stress and strain before failure. In addition to these primary mechanical properties, Poisson's ratio (υ) was calculated based on the strain distribution, providing insights into the lateral deformation behavior of the laminate under tensile stress. Poisson's ratio complements the stress-strain data by describing the material's elastic response, specifically the relationship between longitudinal and lateral strain. Together with the yield stress and ultimate tensile strength, Poisson's ratio serves as an essential output feature for this study, as these properties offer a comprehensive understanding of the laminate's mechanical performance under tensile loading.

The dataset for training process consisted of 230 samples, each representing a unique combination of input parameters and their corresponding mechanical responses. To ensure a comprehensive and diverse dataspace, the dataset was generated using a hybrid sampling approach. This approach combined stratified sampling, random sampling, and edge-case augmentation in the following way: First, stratified sampling was used to divide the input parameters into distinct groups or strata. Samples were then drawn proportionally from each stratum to ensure balanced representation across these key parameters. Next, random sampling was applied within each stratum to introduce variability and ensure that no specific parameter combination was over-represented. Finally, edge-case augmentation was incorporated to explicitly include extreme values for critical parameters,, ensuring that the dataset covers the full range of possible processing conditions and material behaviors. This hybrid approach allowed for a well-distributed and diverse dataset, capturing the full spectrum of mechanical responses while preventing bias towards any single set of conditions. To prepare the dataset for ML training, all input and output features were normalized to a range of 0 to 1. This preprocessing step ensured that all features contributed equally to the training process, preventing features with larger numerical ranges from dominating the learning process. The careful selection of input and output features, combined with systematic dataset generation and normalization, ensured that the ML model was trained on a robust and representative dataset. By incorporating both process parameters and mechanical responses, the dataset captured the relationships between the hot pressing conditions, material behavior, and final mechanical properties of the Ti/Al/Ti laminates.

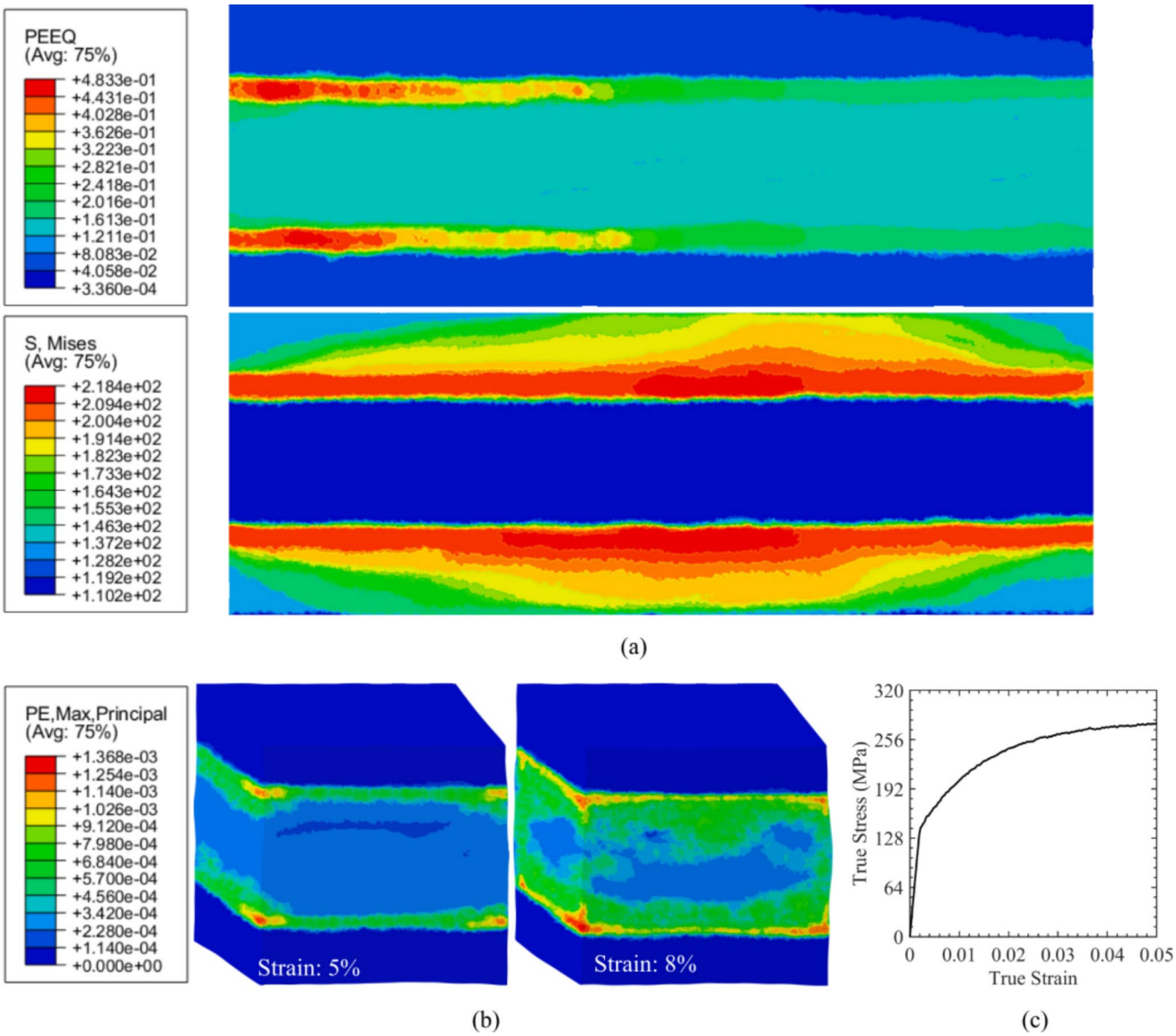

Fig. 2 An example illustrating: (**a**) stress and strain maps in pressed samples, (**b**) strain maps for RVE samples during tensile testing, and (**c**) stress-strain curves

2.3 ML implementation

In this study, ML models were implemented with a focus on the Random Forest (RF) algorithm, which was chosen for its robustness to overfitting, scalability, and ability to handle complex, nonlinear relationships. RF builds an ensemble of decision trees, aggregating their outputs to improve stability and accuracy [32, 33]. This makes it particularly well-suited for analyzing the intricate interplay of mechanical properties in laminates. To further enhance its predictive performance, three distinct hyperparameter tuning methods—Grid Search (GS), Particle Swarm Optimization (PSO), and Genetic Algorithm (GA)—were systematically employed. Each method was designed to effectively navigate the parameter space and identify optimal configurations that maximize model accuracy. The details of these methods, integral to the RF structure (see Fig. 3), are described as follows:

A. **Grid Search Optimization for RF Tuning**: To enhance the predictive accuracy of the RF model in analyzing the mechanical behavior of Ti/Al/Ti laminates, Grid Search (GS) was employed for systematic hyperparameter optimization. Grid Search is an exhaustive tuning technique that explores a predefined grid of hyperparameter values to identify the optimal configuration [34]. Key hyperparameters tuned included the number of trees (N_{trees}), maximum tree depth (D_{max}), and minimum number of samples required to split an internal

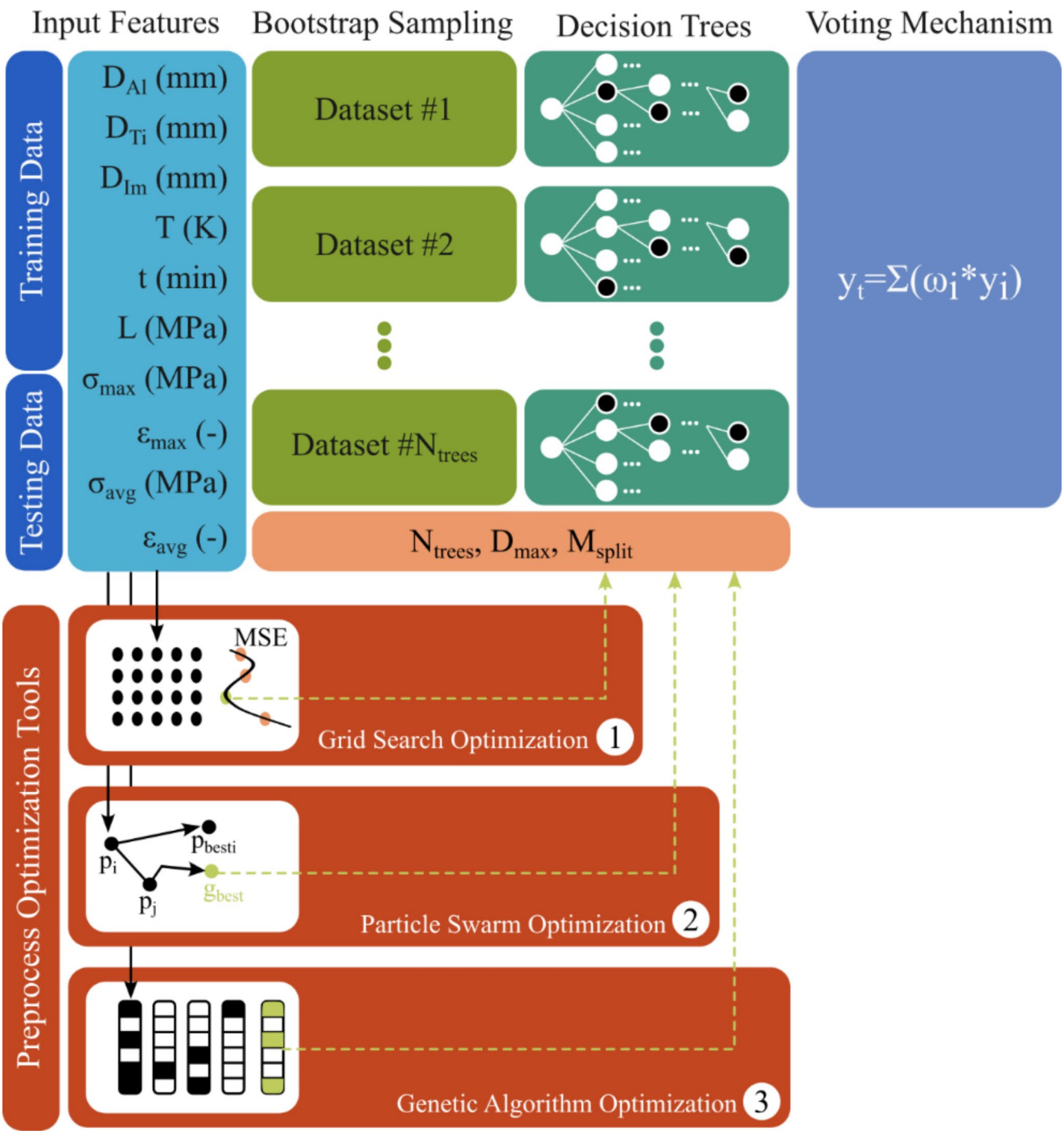

Fig. 3 Structure of the Random Forest model with various hyperparameter tuning processes

node (M_{split}). By systematically varying these parameters within specified ranges, the model's performance was evaluated through cross-validation.

B. The performance metric, mean squared error (MSE), is expressed as:

$$MSE = \frac{1}{N}\sum_{i=1}^{N}(y_i - \dot{y}_i)^2 \quad (1)$$

Where y_i represents the true values, $\dot{y}_i$ the predicted values, and N the number of samples. Alternatively, the coefficient of determination (R^2) was also considered. Grid Search identifies configurations that minimize MSE or maximize R^2, ensuring the RF model is fine-tuned for high predictive accuracy.

C. **PSO for RF Tuning**: The RF model was further optimized using Particle Swarm Optimization (PSO) to enhance its predictive accuracy in analyzing the mechanical behavior of Ti/Al/Ti laminates. PSO is an iterative optimization algorithm inspired by the social behavior of birds flocking or fish schooling. It optimizes hyperparameters by simulating a swarm of particles, each representing a potential solution [35, 36]. In this study, the key RF hyperparameters optimized using PSO included the number of trees, maximum depth, and the minimum samples required to split a node. The process begins with a randomly initialized population of particles, each exploring the hyperparameter space. The fitness of each particle is evaluated using the model's performance, measured by the MSE. The particles' positions are updated according to the velocity formula:

$$v_i\left(t+1\right) = wv_i\left(t\right) + c_1 r_1\left(p_i - x_i\right) + c_2 r_2 (g_i - x_i) \tag{2}$$

Where $v_i(t)$ is the velocity of particle i at time t, x_i is the current position (hyperparameter values), p_i is the best position, g_i is the global best position, c_1 and c_2 are acceleration coefficients, and $r_1$and r_2 are random values between [0, 1]. The new position of the particle is then updated using:

$$x_i\left(t+1\right) = x_i\left(t\right) + v_i(t+1) \tag{3}$$

PSO iterates over generations, updating particle positions and velocities until convergence, at which point the optimal hyperparameters for the RF model are identified. This process significantly enhances the RF model's performance in predicting the mechanical behavior of Ti/Al/Ti laminates.

C) **GA Optimization for RF Tuning**: The RF model was also optimized using a Genetic Algorithm (GA) to enhance its predictive performance for analyzing materials properties. GA is an evolutionary search heuristic inspired by natural selection. It mimics biological evolution through selection, crossover, and mutation to explore the hyperparameter space and identify the optimal values for the RF model [37, 38]. Initially, a population of individuals, each representing a potential combination of hyperparameters, is created. In this study, the hyperparameters optimized by GA included the number of trees, maximum depth, and minimum samples required to split a node, with these values encoded as chromosomes. The fitness of each individual is evaluated based on the RF model's performance, typically defined as the inverse of the MSE. Selection is based on fitness, with higher-probability reproduction for individuals that perform better, as indicated by the formula:

$$P\left(x_i\right) = \frac{Fitness\left(x_i\right)}{\sum_{k=1}^{Npop} Fitness\ \left(x_k\right)} \tag{4}$$

Next, crossover combines genes from two parent solutions at a crossover point c, as shown by:

$$\begin{cases} Offspring_1 = [Parent_1\left[1:c\right], Parent_2[c+1:n]] \\ Offspring_2 = [Parent_2\left[1:c\right], Parent_1[c+1:n]] \end{cases} \tag{5}$$

Mutation introduces diversity by slightly altering genes using a random perturbation:

$$Chromosome_i\left[j\right] = Chromosome_i\left[j\right] + \epsilon \tag{6}$$

Where ε represents a random perturbation. Elitism is also employed to retain the best individuals across generations, ensuring that the optimal solutions are preserved. These steps are repeated for G_{max} generations or until convergence, which is achieved when minimal change in fitness values is observed. This structured approach explores the hyperparameter space effectively, resulting in a robust and well-optimized RF model.

2.4 Results and discussion

Before proceeding with the characterization and evaluation of the machine learning models, it is important to justify the selection of 230 samples for the dataset and assess whether this sample size is adequate for the training process. Figure 4 exhibits the relationship between dataset size and MSE for the ML models, with the convergence curves indicating the performance of each model. As shown in the figure, for both the GS- and PSO-based models, the convergence curves stabilize within the range of 220–230 samples, suggesting that further increases in sample size do not significantly improve model performance. In contrast, for the GA-based model, the convergence occurs slightly earlier, within the range of 200–215 samples, where the MSE reaches its minimum value. These findings support the selection of 230 samples as the final dataset size, ensuring that the data sufficiently captures the underlying patterns while striking an optimal balance between model accuracy and computational efficiency, thereby delivering reliable and stable results for subsequent analysis.

Figure 5 illustrates the relationship between the number of input features and the models' prediction performance, highlighting the efficiency of each method in utilizing input data. As can be seen, the GS-based model requires the full set of input features to achieve its peak prediction performance. This is expected, as GS systematically evaluates all possible hyperparameter combinations without prioritizing specific features, making it reliant on the complete dataset to ensure optimal results. In contrast, the PSO-based model demonstrates a more selective approach. For predicting yield and ultimate strengths, PSO achieves maximum accuracy using

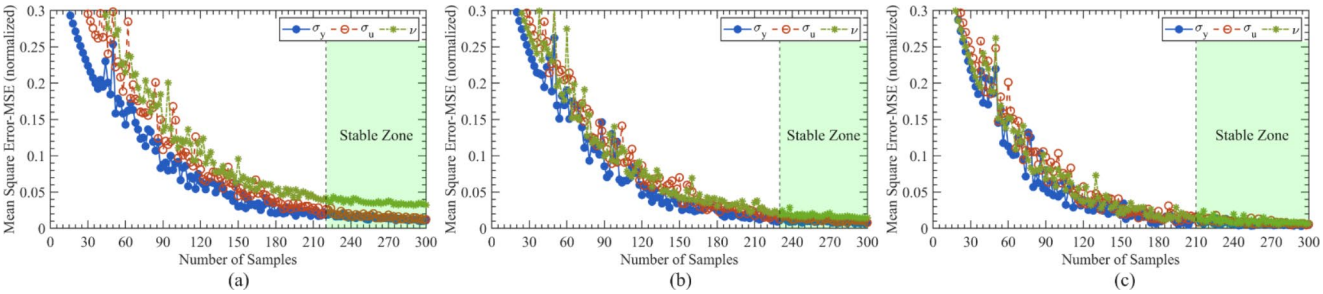

Fig. 4 Relationship between dataset size and MSE in the models tuned by (**a**) Genetic Algorithm, (**b**) Particle Swarm Optimization, and (**c**) Grid Search

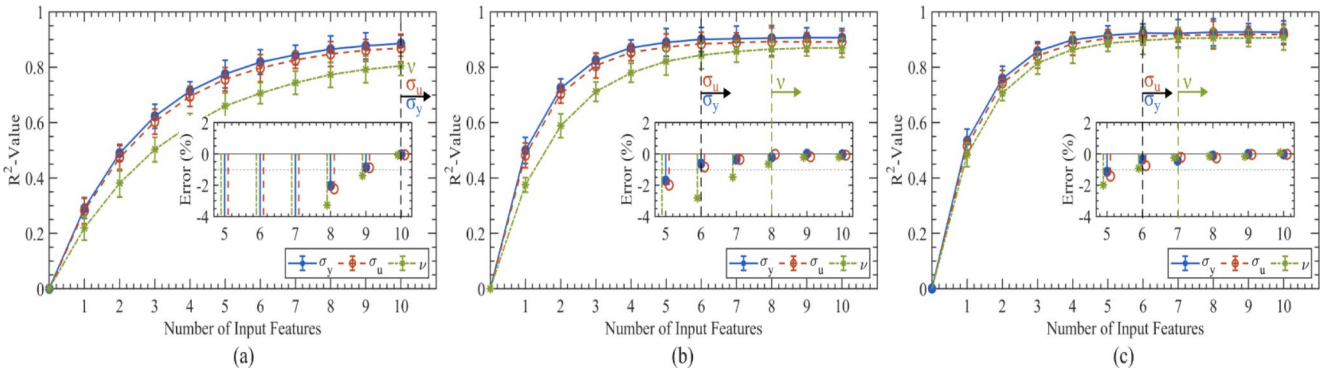

Fig. 5 Feature selection for Random Forest models tuned using: (**a**) Grid Search, (**b**) Particle Swarm Optimization, and (**c**) Genetic Algorithm

only the material thickness and process parameters. However, for Poisson's ratio prediction, the model also incorporates maximum and average strain features. This behavior reflects PSO's capability to identify the most impactful features for each output variable, leveraging its dynamic exploration and exploitation mechanisms to minimize redundant inputs. The GA-based model further refines feature utilization, achieving optimal predictions with the least number of features. For yield and ultimate strengths, similar to PSO, GA requires only the material thicknesses and process parameters. For Poisson's ratio, the model needs just one additional feature: average strain. GA's global search capabilities, coupled with evolutionary operations, enable it to prioritize features that contribute most significantly to model performance while disregarding less relevant inputs.

Figure 6 represents contour plots that illustrate the results of hyperparameter tuning for three RF models, optimized using GS, PSO, and GA. The hyperparameters optimized in this study are constrained to integer values, making the optimization problem non-convex. To address this, we adapted each optimization method to handle discrete variables effectively. For GS, an exhaustive search was performed over a predefined grid of integer values. By systematically evaluating all possible combinations, GS ensures that the optimal integer-valued configuration is identified, even in the presence of a non-convex optimization landscape. For PSO, particle positions were rounded to the nearest integer after each update. This adaptation allows PSO to explore the discrete search space dynamically while maintaining its ability to navigate complex, non-linear relationships. The velocity and position update rules (Eqs. 2 and 3) were applied as usual, but the final positions were constrained to integer values, ensuring that the hyperparameters remain valid for the RF model. For GA, the hyperparameters were encoded as integer-valued genes in the chromosomes. Crossover and mutation operations were designed to preserve the integer nature of the variables. During crossover, offspring chromosomes inherited integer values from their parents, while mutation introduced small integer perturbations to the genes. This approach allows GA to effectively explore the discrete search space and converge to near-optimal solutions, leveraging its global search capabilities to escape local optima. As can be seen in Fig. 6, the tuning process focused on three critical hyperparameters: N_{trees}, D_{max}, and M_{split}. The plots offer insights into the optimal configurations for each hyperparameter combination, resulting in the best model performance for the output variables. For Grid Search, the results show that the optimal number of trees ranged from 100 to 120 for most output variables, striking a balance between computational efficiency and model performance. This range reflects GS's exhaustive search through predefined hyperparameter grids, which is well-suited for finding reliable, moderate values that balance performance and computational cost. For maximum depth, the optimal range was

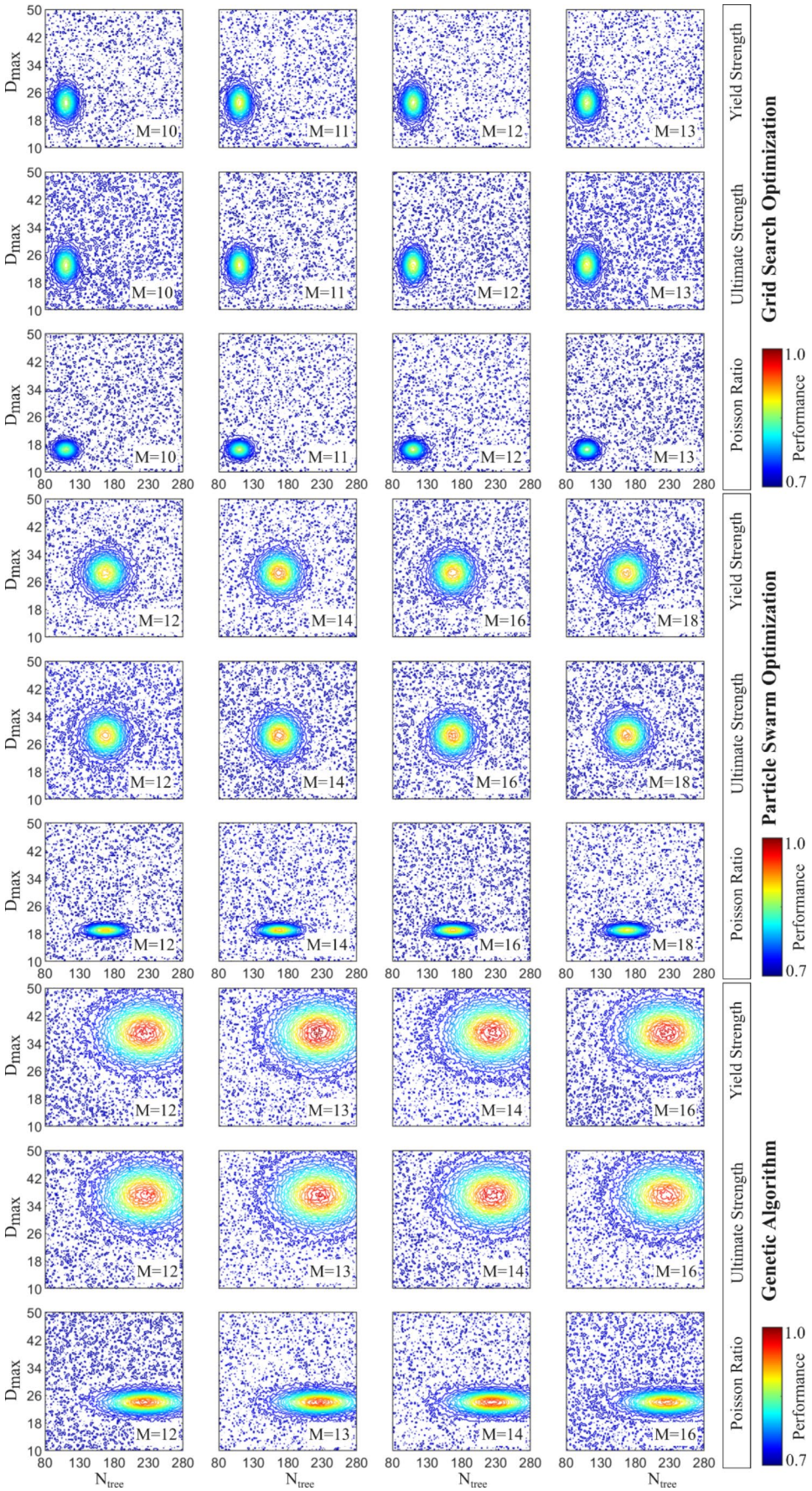

Fig. 6 2D contour plots illustrating hyperparameter optimization using different methods

found to be 20 to 26 for both σ_y and σ_u, while for ν, a more conservative depth of 15 to 18 was preferred. This lower depth for Poisson's ratio helps avoid overfitting by limiting tree complexity. Moreover, the M_{split} was most effective in the range of 10 to 12 samples, ensuring sufficient data for splitting while preventing overfitting. In contrast, the PSO provided more refined hyperparameter choices. The optimal N_{trees} range increased to 150 to 185 trees, reflecting PSO's ability to navigate a broader solution space and fine-tune the model's complexity. For maximum depth, the optimal range was 25 to 32 for both σ_y and σ_u, allowing the model to capture more precise patterns in the data. For Poisson's ratio, a slightly lower range of 18 to 20 for D_{max} helped maintain the model's ability to generalize while capturing necessary complexities. The M_{split} parameter in PSO was most effective in the range of 12 to 16 samples, achieving a balance between model accuracy and generalizability. On the other hand, GA optimization presented the most significant variation in hyperparameter values, with the highest performance achieved for N_{trees} in the range of 190 to 260 trees, particularly for σ_u, where the larger number of trees was essential to identify intricate non-linear relationships. For D_{max}, the optimal range was 32 to 42 for both σ_y and σ_u, allowing the trees to model deeper interactions within the data without overfitting. For Poisson's ratio, GA favored a range of 22 to 26 for D_{max}, ensuring robust generalization while maintaining complexity. The M_{split} values in the GA-optimized plots were also found to be effective between 12 and 16 samples, contributing to strong model performance without excessive data splitting. The higher values for the GA are attributed to its global search and evolutionary processes, which involve mutation and crossover. Unlike more localized search methods such as GS and PSO, GA starts with a random population and progressively evolves towards optimal solutions [39]. This allows it to explore a wider range of hyperparameter configurations, often leading to higher values as it seeks more complex or powerful configurations that may provide better performance for the dataset. The ability to explore this broader solution space enables GA to identify intricate relationships in the data, making it well-suited for capturing complex patterns.

Figure 7 exhibits the convergence behaviors of ML models under different hyperparameter tuning processes. The outcomes aim to show how the optimization process improves model performance over time as the algorithms explore different hyperparameter configurations. Before examining the results, it is worth mentioning that in the grid search method, iterations primarily highlight the effect of reducing the grid size on the final prediction performance. In contrast, iterations in PSO and GA represent the progression of the optimization process, incorporating new variations and adaptive mechanisms to refine the search for optimal hyperparameter configurations. The results indicate that the GS exhibits a relatively steady improvement in performance, but it shows a slower convergence rate compared to PSO and GA. This is because GS performs an exhaustive search over a predefined grid of hyperparameters, evaluating each combination systematically [40]. Since GS relies on a fixed grid, it cannot dynamically adapt or explore the solution space in the same way as PSO or GA. As a result, the convergence curve for GS typically starts with moderate performance and then progresses steadily. The algorithm reaches its optimal performance after a fixed number of iterations, typically within 90 to 120 evaluations, corresponding to the number of grid combinations it must check. This makes GS more methodical but slower in reaching the optimal solution.

PSO method, on the other hand, demonstrates faster convergence compared to GS. PSO is a population-based optimization algorithm, where particles explore the solution space dynamically, adjusting their positions based on the best solutions found by the swarm. The convergence curve for PSO typically shows rapid improvement during the early iterations (~ 70), followed by a stabilization (damped) phase as the particles refine the best solutions. PSO's ability to explore a broader range of hyperparameter values gives

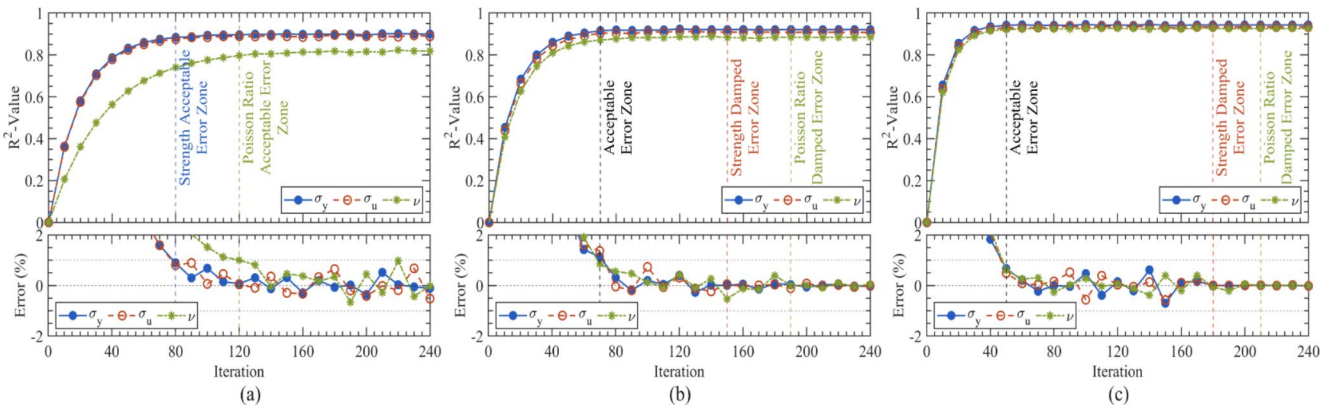

Fig. 7 Model performance trends over iterations through using: (**a**) Grid Search, (**b**) Particle Swarm Optimization, and (**c**) Genetic Algorithm

it an edge in finding near-optimal solutions more quickly. Optimal performance is generally reached within 150 to 190 iterations, depending on the complexity of the problem and the search space. Finally, the GA shows the fastest convergence among the three methods, with the most pronounced improvements during the early iterations. The convergence curve for GA often exhibits rapid progress, particularly in the first 50 iterations, followed by a deceleration as the algorithm focuses on narrowing down the optimal solution. The GA algorithm's global search capability enables it to escape local minima and identify better solutions. In this case, optimal performance is typically reached within 180 to 210 iterations, reflecting GA's ability to refine solutions progressively. In conclusion, it is important to note that while the GA model requires more iterations due to its complexity, its steady-state error is lower compared to other models.

Figure 8 presents the results of regression analysis, depicted as deviation data, highlighting the prediction performance of the GS, PSO, and GA models for yield stress, yield strength, and Poisson's ratio. For the GS model, the R^2 values for yield stress, yield strength, and Poisson's ratio are 0.901, 0.895, and 0.823, respectively. The PSO model demonstrates slightly improved performance, with R^2 values of 0.923 for yield stress, 0.912 for yield strength, and 0.888 for Poisson's ratio. The GA model outperforms both, achieving R^2 values of 0.947 for yield stress, 0.937 for yield strength, and 0.928 for Poisson's ratio. These results clearly indicate that all models exhibit better predictive accuracy for yield stress and yield strength compared to Poisson's ratio. The disparity in prediction accuracy can be attributed to the intrinsic characteristics of the mechanical properties. Yield stress and yield strength are directly influenced by material and process parameters, making them more straightforward for the models to capture. Conversely, Poisson's ratio is a more intricate property, reflecting the material's elastic and deformation behavior, which involves more complex relationships and dependencies [41]. As a result, Poisson's ratio is more challenging for the models to predict accurately. Analyzing the GS model, signs of underfitting (bias) are evident, particularly in predicting Poisson's ratio. This underfitting arises from the rigid nature of the grid search method, which systematically explores a predefined set of hyperparameters. While effective for structured exploration, this approach lacks the flexibility to adapt dynamically to complex, non-linear relationships within the data. Consequently, the GS model struggles with properties like Poisson's ratio,

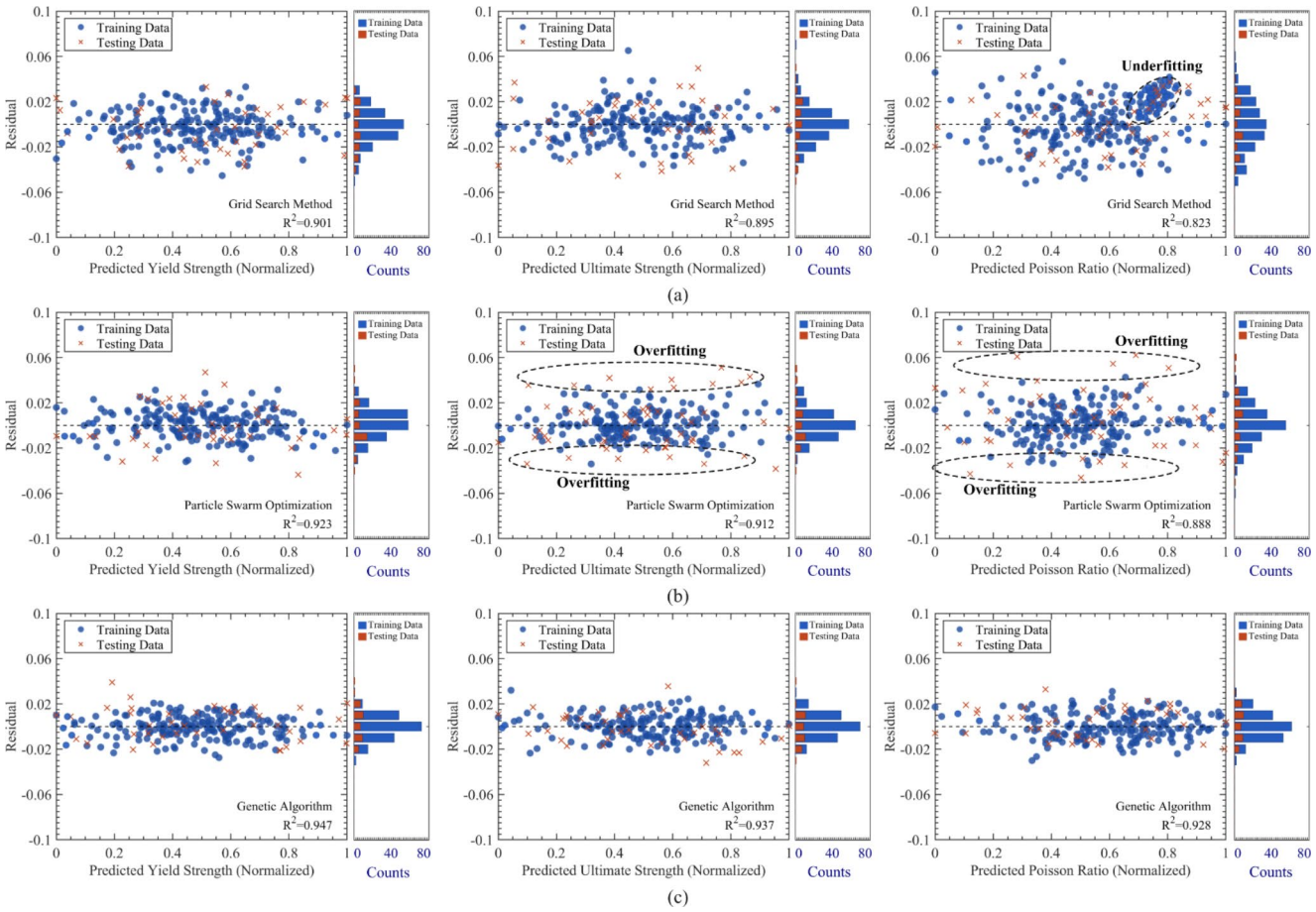

Fig. 8 Data deviation in predictions for models tuned using: (**a**) Grid Search, (**b**) Particle Swarm Optimization, and (**c**) Genetic Algorithm

which demand greater representational capacity. In contrast, the PSO model shows signs of overfitting, especially for yield strength and Poisson's ratio. The PSO algorithm's ability to explore a wide range of hyperparameters and refine its search dynamically can sometimes lead to excessive focus on the training data [42, 43]. This overfitting is particularly evident in scenarios with limited training datasets or insufficient regularization mechanisms, where the model prioritizes training performance at the expense of generalization. Finally, the GA model demonstrates no significant signs of underfitting or overfitting, delivering the most robust performance across all outputs. This superior balance is attributed to GA's evolutionary approach, which combines global exploration with mechanisms like crossover and mutation to escape local minima and thoroughly explore the solution space. This ability ensures consistent and accurate predictions, even for more complex properties like Poisson's ratio, making the GA model the most effective among the three.

Figure 9 presents the mean feature importance analysis of RF models for all output targets. The feature importance values were calculated using permutation importance, a robust method that evaluates the contribution of each feature to the model's predictive performance [44, 45]. This process involves permuting the values of each feature individually and measuring the resulting increase in the model's prediction error. To facilitate meaningful comparisons, the feature importance values were normalized so that their sum equals 1, allowing for a clear and interpretable assessment of the relative contributions of each feature. Moreover, one should note that the input features analyzed in this figure align with those depicted in Fig. 5, ensuring consistency across the analyses. The results reveal distinct patterns in how different features influence model performance across the three optimization methods: GS, PSO, and GA. In the GS-based model, the processing parameters of pressing and material thickness exhibit the highest impact on predicting yield stress and ultimate strength. These features dominate the model's performance, underscoring their direct influence on the material's mechanical behavior. Conversely, for Poisson's ratio predictions, strain- and stress-related input features take precedence, collectively accounting for 0.33 of the feature importance. This shift suggests that Poisson's ratio depends more on deformation-specific characteristics rather than bulk material properties, highlighting the GS model's focus on fundamental relationships. On the other hand, the PSO-based model shows a different pattern. For yield stress and ultimate strength predictions, the processing parameters and material thickness remain dominant, with the former contributing the largest share. However, for Poisson's ratio, strain-related features, particularly ε_{max} and ε_{ave}, emerge as the most significant, collectively contributing over 0.35 of the total feature importance. This highlights the heightened sensitivity of Poisson's ratio to strain characteristics in the PSO model, likely reflecting the algorithm's capability to emphasize features that capture complex, non-linear dependencies. However, this tendency may also heighten the risk of overfitting, particularly without sufficient regularization. Finally, the GA-based model demonstrates a balanced contribution of material thickness and processing parameters for predicting yield stress and ultimate strength. This balance reflects the GA model's ability to explore and integrate diverse feature interactions effectively. For Poisson's ratio, only one strain-related feature, ε_{ave}, is found to be significant, contributing 0.17 of the total feature importance. This focused reliance suggests that the GA model efficiently identifies the most relevant input for Poisson's ratio prediction while maintaining a balanced approach for strength predictions. Comparing the PSO and GA models provides further insights. The GA model's balanced feature contributions for yield stress and ultimate

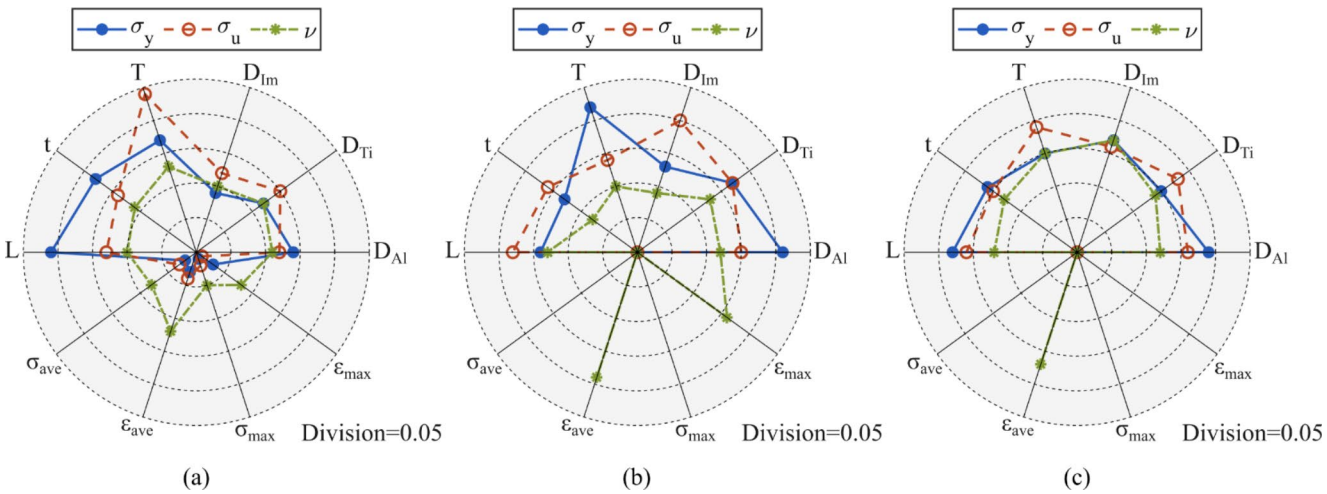

Fig. 9 Mean relevance scores of input features for achieving the highest predictive performance with the Random Forest model tuned using: (**a**) Grid Search, (**b**) Particle Swarm Optimization, and (**c**) Genetic Algorithm

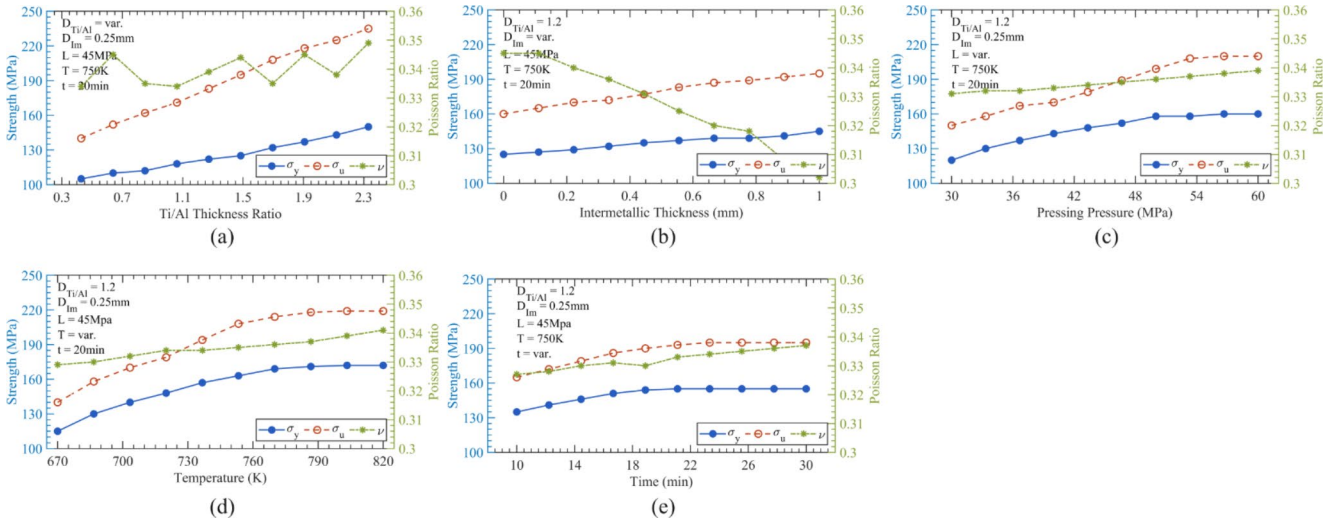

Fig. 10 A case study illustrating the relationships between: (**a**) $D_{Ti/Al}$, (**b**) intermetallic thickness, (**c**) pressing pressure, (**d**) pressing temperature, and (**e**) pressing time with the mechanical properties (output targets), while keeping other parameters constant

strength predictions, combined with its targeted emphasis on a single strain-related feature for Poisson's ratio, demonstrate its robust exploration and optimization capabilities. In contrast, the PSO model's greater reliance on strain features for Poisson's ratio highlights its optimization-driven ability to capture complex relationships. However, this focus may also increase susceptibility to overfitting, emphasizing the need for careful mitigation strategies when using PSO.

In the final step, the GA-based ML model, identified as the most accurate predictor in this study, enables a comprehensive analysis of how processing and geometrical parameters influence the mechanical properties of laminated samples. As illustrated in Fig. 10a, increasing the Ti/Al thickness ratio results in a significant rise in both yield stress and ultimate tensile strength of the laminates. Notably, the rate of increase in σ_u is higher than that of σ_y, which suggests that the increasing proportion of Ti enhances the laminate's work-hardening capacity, thereby contributing more significantly to strength [46, 47]. This is consistent with the mechanical properties of Ti, which exhibit superior strength and work hardening compared to Al. The increased Ti content causes a higher resistance to plastic deformation, thus improving the laminate's overall strength. In contrast, the Poisson's ratio remains relatively stable within a narrow range (0.334–0.349), indicating that changes in the base metal thicknesses have little effect on the laminate's deformation behavior under uniaxial loading. This stability can be attributed to the similar Poisson's ratios of Ti (~0.34) and Al (~0.33), meaning that variations in their thicknesses do not significantly alter the laminate's overall lateral deformation characteristics. Turning to the influence of intermetallic layer thickness, Fig. 10b shows that increasing the intermetallic thickness leads to a proportional increase in both σ_y and σ_u. However, the rate of increment is similar for both properties, indicating that the intermetallic layer does not contribute significantly to the laminate's work-hardening behavior, contrary to what is observed in Fig. 10a. This is consistent with the typically brittle nature of intermetallics, which have lower ductility compared to Ti and Al. In the simulations, intermetallics are typically modeled as materials with limited plasticity, acting more as stiffening agents rather than enhancing the laminate's ability to undergo plastic deformation. As a result, the increase in intermetallic thickness strengthens the laminate but does not notably increase its work-hardening capacity. On the other hand, the Poisson's ratio tends to decrease with increasing intermetallic thickness, reflecting the restricted lateral expansion of the laminate due to the brittle nature of the intermetallics. This results in reduced deformation in the transverse direction compared to the more ductile base metals. The effects of pressing parameters— pressing pressure, pressing temperature, and pressing time—are also depicted in Fig. 10c and d, and 10e. The results indicate that increasing the pressing pressure enhances material densification and improves the uniformity of pressure distribution within the laminate. This leads to better interfacial bonding between the layers, resulting in higher σ_y and σ_u. The most significant improvement is observed in ultimate strength, which is directly tied to the reduction of any delamination or defects at the interfaces, ensuring a more even stress distribution under load. Similarly, elevated pressing temperatures promote better thermal activation, facilitating improved flow at the interfaces, which strengthens the bonding between the Ti and Al layers. The results also show that increasing pressing time leads to further improvements in bonding, yielding stronger laminates with superior mechanical properties. However, these

effects reach a saturation point once material densification and interfacial bonding become stable. Hence, beyond certain thresholds of pressing pressure, temperature, or pressing time, further increases do not significantly enhance the laminate's mechanical properties. The reason for this is that once the materials are sufficiently densified and the interfaces are fully bonded, additional processing does not result in substantial improvements [9, 48]. This is especially true for the pressing time, which, after a certain duration, primarily serves to solidify the bond, while further increases add minimal benefit. Moreover, it can be observed that the effects of pressing pressure and pressing temperature are significantly higher than pressing time. This is because pressing pressure directly influences the densification and uniformity of the laminate, while pressing temperature accelerates the material flow and interface bonding, both of which are critical for achieving high mechanical strength. Pressing time, on the other hand, primarily influences the steady-state bonding process, which becomes less impactful after a certain threshold. Finally, it is noteworthy that the increase in the mentioned parameters leads to a slight increment in Poisson's ratio, which can be attributed to the improved interfacial bonding. As the laminate becomes more compact and the interfaces more robust, the laminate's ability to deform laterally slightly increases, leading to a small rise in Poisson's ratio. However, this change is minimal and does not significantly affect the overall deformation behavior due to the dominance of the base material properties.

3 Conclusions

This study proposed a machine learning approach using GA-tuned RF model to predict the mechanical properties of hot-pressed Ti/Al/Ti laminates. The main outcomes are as follows:

(a) The model demonstrated outstanding predictive capabilities, with R^2 values of 0.947 for yield stress, 0.937 for ultimate strength, and 0.928 for Poisson's ratio. These results highlight the model's robustness and its capacity to accurately capture the complex mechanical behaviors of Ti/Al/Ti laminates.

(b) The GA-tuned RF model outperformed Grid Search (GS) and Particle Swarm Optimization (PSO) by effectively optimizing key hyperparameters, including N_{trees}, D_{max}, and M_{split}). Specifically, the optimal ranges for N_{trees} (190–260) and D_{max} (32–42 for σ_y and σ_u, and 22–26 for ν) enabled the model to balance complexity and generalization effectively, capturing intricate nonlinear relationships without overfitting. Moreover, for M_{split}, an optimal range of 12–16 samples ensured strong performance without excessive data fragmentation.

(c) The GA-tuned RF model revealed key relationships between material geometries (e.g., laminate thicknesses) and pressing parameters for σ_y and σ_u, while induced strain emerged as a significant contributor in predicting ν.

(d) The GA-based model accurately analyzed the effects of processing and geometrical parameters on Ti/Al/Ti laminates. Increasing the Ti/Al thickness ratio improved σ_y and σ_u, while Poisson's ratio remained stable. Thicker intermetallic layers strengthened laminates but reduced lateral deformation. Pressing pressure and temperature had the most significant effects, enhancing densification and bonding, while pressing time showed diminishing returns beyond critical thresholds.

Acknowledgements The authors extend their appreciation to King Saud University for funding this work through Researchers Supporting Project number (RSPD2025R704), King Saud University, Riyadh, Saudi Arabia.

Author contributions M. S., N. R., and T. R. contributed to modeling and investigation, while M. S. and A. S. were responsible for conceptualization. A. S., V. S. M., and M. M. were involved in data analysis and curation. All authors participated in the preparation of the manuscript.

Data availability The data that support the findings of this study are available on reasonable request.

Declarations

Conflict of interest Authors declare that they have no conflicts of interest.

References

1. P. Zhou, M. Yuan, M. Jia, X. Pei, Y. Wang, W. Yang, H. Wang, Y. Zhao, New strategy for enhancing the strength and toughness of Ti-Al metallic-intermetallic laminated composites: constructing multiple heterostructures using Ni foil. Prog Nat. Sci. Mater. Int. **34**, 1173–1183 (2024)
2. Y. Wang, X. Liu, W. Zhang, Analysis on the mechanism of titanium plate pretreated by ultrasonic shot peening in improving interfacial shear strength of Ti/Al laminated composite. Mater. Sci. Eng. A **917**, 147393 (2024)
3. M. Lipińska, E. Ura-Bińczyk, S. Mróz, Z. Szulc, A. Stefanik, P. Szota, M. Lewandowska, Microstructure and corrosion resistance of Ni-Ti-Al multi-layer laminates manufactured by explosive welding with subsequent rolling. J. Manuf. Process. **105**, 84–98 (2023)
4. Y. Zhang, Z. Su, D. Zhang, Z. Zhu, Microstructural and mechanical property analyses of Ti/Al/Ti laminated composites prepared by ultrasonic welding. Mater. Res. **27**, e20230538 (2024)
5. W. Zhang, Y. Wang, X. Liu, Enhancing interface bonding strength of Ti/Al laminated composites via periodic surface nano-crystallization pretreatment. Mater. Sci. Eng. A **901**, 146560 (2024)

6. M.R. Karimi, K. Abrinia, K.M. Hamdia, S.M. Hashemianzadeh, M. Baniassadi, Effects of functional group type and coverage on the interfacial strength and load transfer of graphene-polyethylene nanocomposites: a molecular dynamics simulation. Appl. Phys. A **128**, 341 (2022). https://doi.org/10.1007/s00339-022-05427-x
7. Y. Wang, J. Du, H. Xiao, Interfacial evolution and coordinated deformation mechanism of Ti/Al laminated metal composites prepared by diffusion bonding. J. Mater. Res. Technol. **27**, 4541–4551 (2023)
8. C. Chen, M. Hu, W. Hong, Comparison of rolling and transverse direction properties of Al/Ti laminated metal composites prepared by cold roll bonding and subsequent annealing, trans. Indian Inst. Met. **77**, 3739–3749 (2024)
9. B. Que, L. Chen, Y. Chen, L. Qian, G. Zhao, C. Zhang, Fabrication of Al/Al-TiB2 laminate composites via hot press sintering process: an insight into the mechanical properties and fracture behavior. J. Manuf. Process. **109**, 53–64 (2024)
10. B. Sariyev, A. Abdikadyr, T. Baitikenov, Y. Anuarbekov, B. Golman, C. Spitas, Thermal properties and mechanical behavior of hot pressed PEEK/graphite thin film laminate composites. Sci. Rep. **13**, 12785 (2023)
11. Z. Huang, L. Meng, P. Lin, X. Cao, Z. Zhang, G. Liu, Formability improvement of hot-pressed Ti/Al laminated sheet by TiAl3 layer growth and crack healing during deformation. J. Alloys Compd. **938**, 168604 (2023). https://doi.org/10.1016/j.jallcom.2022.168604
12. B. Que, L. Chen, L. Qian, X. Kong, G. Zhao, Tailoring the microstructure of Al/Ti laminated composite through hot press sintering process to achieve superior mechanical properties. J. Mater. Process. Technol. **326**, 118349 (2024). https://doi.org/10.1016/j.jmatprotec.2024.118349
13. B. Que, L. Chen, Y. Zhao, L. Qian, J. Lin, C. Zhang, G. Zhao, Hierarchical modification of bimodal grain structure in Al/Ti laminated composites for extraordinary strength-ductility synergy. Compos. Part. Appl. Sci. Manuf. **187**, 108438 (2024). https://doi.org/10.1016/j.compositesa.2024.108438
14. C. Guo, H. Shi, S. Wang, F. Jiang, T. Dong, X. Jing, Microstructure characterization and mechanical properties of the NiTif-Reinforced Ti/Al-Laminated composites using vacuum hot pressing with ultrasonic consolidation assisted. Adv. Eng. Mater. **26**, 2400041 (2024). https://doi.org/10.1002/adem.202400041
15. E. Wang, L. Lv, F. Kang, N. Hu, F. Jiang, J. Li, W. Jiang, Y. Cao, Microstructure and bending behavior of Ti/Al laminated composites reinforced with high-entropy alloy particles. J. Mater. Res. Technol. **27**, 7495–7505 (2023). https://doi.org/10.1016/j.jmrt.2023.11.189
16. H. Ma, R.S. Pierce, J. Beauson, Optimisation of process-induced residual stresses in composite laminates by different genetic algorithm and finite element simulation coupling methods. J. Compos. Mater. **58**, 2531–2544 (2024)
17. H. Cheng, Z. Zhang, M. Ren, H. Jia, Experimental and numerical simulation studies on V-shaped bending of Aluminum/CFRP laminates. Mater. (Basel). **16**, 4939 (2023)
18. N. Firouzi, K.K. Żur, M. Amabili, T. Rabczuk, On the time-dependent mechanics of membranes via the nonlinear finite element method. Comput. Methods Appl. Mech. Eng. **407**, 115903 (2023). https://doi.org/10.1016/j.cma.2023.115903
19. N. Firouzi, K.K. Żur, On the generalized nonlinear mechanics of compressible, incompressible, isotropic, and anisotropic hyperelastic membranes. Int. J. Solids Struct. **264**, 112088 (2023). https://doi.org/10.1016/j.ijsolstr.2022.112088
20. Z. Li, A. Alkhayyat, A. Yadav, M. Samavatian, V. Samavatian, Elastic constant analysis of orthotropic steel sheets using multitask machine learning and the impulse excitation technique. Phys. Scr. **100**, 16014 (2025). https://doi.org/10.1088/1402-4896/ad9d9e
21. X. Geng, L.-W. Wang, X. Meng, Exploring the strength-concentration relationship of MgCu bioalloys at low copper content using machine learning force fields. Comput. Mater. Sci. **246**, 113486 (2025)
22. A. Valizadeh, R. Sahara, M. Souissi, Alloys innovation through machine learning: a statistical literature review. Sci. Technol. Adv. Mater. Methods. **4**, 2326305 (2024)
23. S. Hiremath, Y. Zhang, L. Zhang, T.-W. Kim, Machine learning approach to evaluating impact behavior in fabric-laminated composite materials. Results Eng. **23**, 102576 (2024)
24. A. Garg, L. Li, W. Zheng, M.-O. Belarbi, R. Raman, Free vibration behaviour of bio-inspired helicoidal laminated composite panels of revolution under thermal conditions: Multi-output machine learning approach. Eng. Anal. Bound. Elem. **169**, 106024 (2024)
25. A. Yadav, N.M. Ghazaly, S. Askar, L.H. Alzubaidi, A.A. Almulla, A.R. Al-Tameemi, Machine learning-powered analysis of hot isostatic pressing for Ti-6Al-4 V powder. Appl. Phys. A **130**, 610 (2024)
26. Z. Yang, M. Yang, R. Sisson, Y. Li, J. Liang, A machine-learning model to predict tensile properties of Ti6Al4V parts prepared by laser powder bed fusion with hot isostatic pressing. Mater. Today Commun. **33**, 104205 (2022)
27. S. Goswami, C. Anitescu, S. Chakraborty, T. Rabczuk, Transfer learning enhanced physics informed neural network for phase-field modeling of fracture, Theor. Appl. Fract. Mech. 106 (2020) 102447. https://doi.org/10.1016/j.tafmec.2019.102447
28. Y. Liu, H.A. Alkhazaleh, M.A. Khan, M. Samavatian, V. Samavatian, Local elasticity assessment of unidirectional fiber-reinforced polymer composites through impulse excitation and machine learning. J. Reinf Plast. Compos. (2024) 07316844241307083
29. E. Samaniego, C. Anitescu, S. Goswami, V.M. Nguyen-Thanh, H. Guo, K. Hamdia, X. Zhuang, T. Rabczuk, An energy approach to the solution of partial differential equations in computational mechanics via machine learning: concepts, implementation and applications, comput. Methods Appl. Mech. Eng. **362**, 112790 (2020). https://doi.org/10.1016/j.cma.2019.112790
30. C. Hammami, N. Kammoun, H. Hentati, M. Ben Amar, M. Haddar, Parametric analysis of the damage characterization tests of aluminum bulk material. J. Mech. Sci. Technol. **36**, 5019–5025 (2022)
31. A.H. Assari, N. Shaghaghi, S. Yaghoobi, S. Ghaderi, Determining the characteristics of representative volume elements in severely deformed aluminum-matrix composite. Heliyon. **10** (2024)
32. W. Zhang, P. Li, L. Wang, X. Fu, F. Wan, Y. Wang, L. Shu, L. Yong, Prediction of the yield strength of as-cast alloys using the random forest algorithm. Mater. Today Commun. **38**, 108520 (2024)
33. A. Nithin, M.J. Davidson, Evaluation of machine learning models for predicting the hot deformation flow stress of sintered Al–Zn–Mg alloy. J. Eng. Mater. Technol. **147**, 21001–21006 (2025)
34. M. Ogunsanya, J. Isichei, S. Desai, Grid search hyperparameter tuning in additive manufacturing processes. Manuf. Lett. **35**, 1031–1042 (2023)
35. Y. Wu, Y. Bai, S. Yang, C. Li, Extracting random forest features with improved adaptive particle swarm optimization for industrial robot fault diagnosis. Measurement. **229**, 114451 (2024)
36. C. Chen, L. Ma, Y. Zhang, P.K. Liaw, J. Ren, Accelerating the design of high-entropy alloys with high hardness by machine learning based on particle swarm optimization. Intermetallics. **154**, 107819 (2023)
37. B.O. Kong, M.S. Kim, B.H. Kim, J.H. Lee, Prediction of creep life using an explainable artificial intelligence technique and alloy design based on the genetic algorithm in creep-strength-enhanced ferritic 9% cr steel. Met. Mater. Int. **29**, 1334–1345 (2023)

38. M. Zhang, C. Zhang, J. Zhang, L. Wang, F. Wang, Effect of composition and curing on alkali activated fly ash-slag binders: machine learning prediction with a random forest-genetic algorithm hybrid model. Constr. Build. Mater. **366**, 129940 (2023)
39. I.D. Raji, H. Bello-Salau, I.J. Umoh, A.J. Onumanyi, M.A. Adegboye, A.T. Salawudeen, Simple deterministic selection-based genetic algorithm for hyperparameter tuning of machine learning models. Appl. Sci. **12**, 1186 (2022)
40. H. Alibrahim, S.A. Ludwig, Hyperparameter optimization: Comparing genetic algorithm against grid search and bayesian optimization, in: 2021 IEEE Congr. Evol. Comput., IEEE, 2021: pp. 1551–1559
41. V.V. Mishakin, V.A. Klyushnikov, A.V. Gonchar, Relation between the deformation energy and the Poisson ratio during Cyclic loading of austenitic steel. Tech. Phys. **60**, 665–668 (2015)
42. M. Clerc, *Particle Swarm Optimization* (Wiley, 2010)
43. D. Wang, D. Tan, L. Liu, Particle swarm optimization algorithm: an overview. Soft Comput. **22**, 387–408 (2018)
44. A. Altmann, L. Toloşi, O. Sander, T. Lengauer, Permutation importance: a corrected feature importance measure. Bioinformatics. **26**, 1340–1347 (2010)
45. S. Janitza, C. Strobl, A.-L. Boulesteix, An AUC-based permutation variable importance measure for random forests. BMC Bioinform. **14**, 1–11 (2013)
46. Y. Du, G. Fan, T. Yu, N. Hansen, L. Geng, X. Huang, Laminated Ti-Al composites: processing, structure and strength. Mater. Sci. Eng. A **673**, 572–580 (2016)
47. M. Cao, C. Wang, K. Deng, K. Nie, W. Liang, Y. Wu, Effect of interface on mechanical properties and formability of Ti/Al/Ti laminated composites. J. Mater. Res. Technol. **14**, 1655–1669 (2021)
48. C. Elibol, S.H. Wapande, Numerical and experimental formability analysis of aluminum 3105 sandwich panels produced by continuous hot-press forming. Mater. Test. **64**, 11–23 (2022)